JOURNAL OF Materials CHEMISTRY

Modification of an ITO anode with a hole-transporting SAM for improved OLED device characteristics†

Jaemin Lee,[a] Byung-Jun Jung,[a] Jeong-Ik Lee,*[b] Hye Yong Chu,[b] Lee-Mi Do[b] and Hong-Ku Shim*[a]

[a]*Department of Chemistry and School of Molecular Science (BK21), Center for Advanced Functional Polymers (CAFPoly), Korea Advanced Institute of Science and Technology (KAIST), 373-1 Guseong-dong, Yuseong-gu, Daejeon 305-701, Republic of Korea. E-mail: hkshim@mail.kaist.ac.kr*

[b]*Basic Research Laboratory, Electronics and Telecommunications Research Institute (ETRI), 161 Gajeong-dong, Yuseong-gu, Daejeon 305-350, Republic of Korea. E-mail: jiklee@etri.re.kr*

Received 16th July 2002, Accepted 2nd September 2002
First published as an Advance Article on the web 4th October 2002

Modification of inorganic electrodes has attracted much attention in the study of organic semiconductor devices. An ethoxysilane functionalized hole-transporting triphenylamine (TPA–CONH–silane) was synthesized and was self-assembled to form a monolayer on an indium tin oxide (ITO) anode. The modified surface was characterized by water contact angle, X-ray photoelectron spectroscopy (XPS), ellipsometry and atomic force microscopy (AFM). The increase in surface work function is expected to facilitate hole injection from the ITO anode. To investigate the effect of a self-assembled monolayer (SAM) on the characteristics an organic light-emitting diode (OLED), a typical OLED device [SAM-modified ITO/TPD (50 nm)/Alq_3 (60 nm)/LiF (1 nm)/Al (70 nm)] was fabricated. The SAM-modified device could endure a higher current and showed a much higher luminance (6300 cd m^{-2}) than the bare ITO device (2700 cd m^{-2}). The external quantum efficiency was also shown to improve as a result of the presence of the SAM. In addition to these device characteristics, a study of the TPD film morphology revealed an enhanced thermal stability for the SAM-modified device. The variation of the terminal group of the SAM and possible further optimization of SAM-modified OLEDs is under investigation.

Introduction

Expertise in electroluminescent organic[1] and polymeric[2] materials and devices has grown progressively during the last decade, notably in the development of high performance organic semiconductors and the optimization of device structures. In particular, from the standpoint of device optimization, it has now been found that the organic/inorganic interface cannot be neglected; although the importance of this interface was missed in the early stages of organic light-emitting diode (OLED) development. Poor adhesion between organic and inorganic electrodes is known to cause device failure[3] and the crystallization of organic films.[4] In the search for improved interfacial contact, a sol–gel process forming hybrid organic–inorganic materials at an indium tin oxide (ITO) anode has been tried.[5–7] Similarly, the use of a high work function oxide anode, which facilitates hole injection, instead of the more commonly used ITO has been reported recently.[8] Therefore modification and development of the inorganic electrode is an active research area.

Self-assembled monolayers (SAMs) are in the limelight as new tools for enhancing the macroscopic bulk properties and microscopic molecular properties of functional materials. SAMs are being studied extensively because of their ease of formation and their wide applicability.[9] It is well known that surface hydroxy groups on the ITO can support a SAM with various kinds of functionalities, such as carboxylic acids,[10] phosphonic acids[11] and silanes.[12,13] Some previous studies report application of a SAM as either a current blocking layer[12] or a moisture penetration blocking layer.[13] Enhanced charge injection as a result of the surface dipolar layer of a SAM has also been reported.[11,14] Schwartz *et al.* reported a similar phenomenon, that variation of the molecular dipole adsorbed on the ITO surface can change the work function of the ITO.[15] Layer-by-layer self-assembly of hole-transporting polymers has been reported to increase the quantum efficiency of the device,[16] and the use of a polyaniline modified ITO electrode for polymer light-emitting diodes (PLEDs) has also been reported.[17] In addition to their use in OLED devices, SAMs with various kinds of surface properties can be applied to molecular electronic devices such as chemical- and biosensors,[18] field-effect transistors (FETs),[19,20] liquid crystal displays (LCDs)[21] and microelectromechanical systems (MEMS).[22]

In this paper we report on the application of a SAM to an ITO anode and report the characteristics of an OLED that makes use of this modified anode. We have introduced a triethoxysilane functionality into the hole-transporting triphenylamine moiety both as constituents of a SAM for application to the hydroxy surfaces. Introduction of a hole-transporting moiety at the end of the SAM is expected to change the surface work function as well as to improve the adhesion between the inorganic ITO and the hole-transporting organic layers.

Experimental

[4-(Diphenylamino)phenyl]methanol (TPA–CH_2OH) was prepared by formylation of triphenylamine through the Vielsmeier reaction[23] followed by reduction of the aldehyde. {[4-(Diphenylamino)phenyl]methoxy}-*N*-(4,4,4-triethoxy-4-silabutyl)-formamide (TPA–CONH–silane) was then obtained by letting

†Electronic supplementary information (ESI) available: 3D structure of TPA–CONH–silane. See http://www.rsc.org/suppdata/jm/b2/b206939c/

 DOI: 10.1039/b206939c

TPA–CH_2OH react with 3-(isocyanatopropyl)triethoxysilane. The crude product was purified by column chromatography, yielding a white powder. This kind of silane synthesis is widely used,[6,18,21] because it is easy to prepare and contains no metal residue, which is seldom able to be removed. In addition, the amide linkage in TPA–CONH–silane is known to improve the ordering of the SAM through interchain hydrogen bonding.[24] Details of the syntheses, surface modification and device experiments are described in the following paragraphs.

Materials

Triphenylamine, phosphorus oxychloride, (3-isocyanatopropyl)triethoxysilane and lithium fluoride were purchased from Aldrich and used without further purification. TPD [*N*′-bis(3-methylphenyl)-*N*,*N*′-diphenyl-1,1′-biphenyl-4,4′-diamine] and Alq_3 [tris-(8-hydroxyquinoline)aluminium] were purchased from TCI and purified by gradient sublimation. Sodium acetate trihydrate, sodium borohydride, sodium hydroxide, triethylamine, pyridine and magnesium sulfate were purchased from Junsei and used without further purification. All other solvents and reagents were analytical-grade quality, purchased commercially and used as received unless otherwise indicated. Anhydrous grade solvents were used during the SAM formation steps.

[4-(Diphenylamino)phenyl]methanol (TPA–CH_2OH)

TPA–CH_2OH was synthesized by reduction of 4-(diphenylamino)benzaldehyde (TPA–CHO) with sodium borohydride ($NaBH_4$). TPA–CHO was prepared using the well-known Vielsmeier reaction according to a literature procedure.[23] 0.290 g (7.60 mmol) of $NaBH_4$ dissolved in 15.0 mL of aqueous 0.1 M NaOH solution was added dropwise into 4.01 g (14.7 mmol) of TPA–CHO in 50.0 mL of ethanol. The mixture was reacted at room temperature for 4 h. The solution was extracted with CH_2Cl_2–H_2O, dried with magnesium sulfate ($MgSO_4$) and then rotary evaporated. Recrystallization with dichloromethane–hexane gave a white solid. The yield was 3.72 g (91.9%). ^{1}H NMR (DMSO-d_6, ppm) δ: 7.21–7.26 (m, 6H), 6.92–6.99 (m, 8H), 5.17 (t, 1H), 4.42 (d, 2H). ^{13}C NMR (DMSO-d_6, ppm) δ: 147.369, 145.858, 137.413, 129.316, 127.822, 123.316, 122.484, 62.658. FT-IR(KBr, cm^{-1}) ν_{max}: 3244.0 (ν_{O-H}).

{[4-(Diphenylamino)phenyl]methoxy}-*N*-(4,4,4-triethoxy-4-silabutyl)formamide (TPA–CONH–silane)

Within a 250 mL two-necked round-bottomed flask, 10.0 g (36.3 mmol) of TPA–CH_2OH was dissolved in 30.0 mL of DMF. 10.3 mL (72.6 mmol) of triethylamine was added to the flask and stirred for a while. Then 8.50 mL (33.0 mmol) of (3-isocyanatopropyl)triethoxysilane was added into the reaction mixture and stirred at 70 °C for 48 h. After cooling to room temperature, the reaction mixture was vacuum concentrated and the product was purified by column chromatography (ethyl acetate : hexane = 1 : 2). Recrystallization with dichloromethane–hexane gave a white solid. The yield was 7.59 g (44.4%). mp 80 °C. ^{1}H NMR ($CDCl_3$, ppm) δ: 7.19–7.25 (m, 6H), 6.99–7.07 (m, 8H), 5.01 (s, 2H), 4.94 (s, 1H), 3.78 (q, 4H), 3.17 (q, 2H), 1.58–1.66 (m, 2H), 1.20 (t, 9H), 0.61 (t, 2H). ^{13}C NMR ($CDCl_3$, ppm) δ: 156.405, 147.701, 147.590, 130.497, 129.303, 129.134, 124.326, 124.019, 123.504, 122.875, 66.254, 58.389, 43.422, 23.255; 18.229, 7.578. FT-IR (KBr, cm^{-1}) ν_{max}: 3340.1 (ν_{N-H}), 1710.0 ($\nu_{C=O}$). EI-MS calcd. for $C_{29}H_{38}N_2O_5Si$ 522.26, found 522.25 (M^+). Anal. (calcd.) C 66.73 (66.64), H 7.78 (7.33), N 5.45 (5.36).

Substrate preparation

Substrates were first cleaned with chloroform, water and then treated with a 7 : 3 solution of concentrated H_2SO_4 and 35% H_2O_2 at 120 °C for 10 min (This acid-treatment step is omitted in the case of the ITO). Then they were treated with a 1 : 1 : 5 solution of NH_4OH, 35% H_2O_2 and H_2O at 80 °C for 20 min. The substrates were then placed in water and finally dried under a stream of dry nitrogen. The cleaned substrates were used immediately upon preparation.

Monolayer characterization

Static water contact angles were measured using a sessile drop goniometer. XPS measurements were made using an ESCALAB 200R X-ray photoelectron spectrometer with a monochromatic Al Kα source. The thickness of the SAM was measured by ellipsometry using an automatic ellipsometer (Rudolph AutoEL-II) equipped with a HeNe laser (623.8 nm). Both the imaginary and the real refractive indices of the silicon wafer were measured prior to self-assembly. The morphologies of the substrates were evaluated by atomic force microscopy (AFM) using an AutoProbe CP (Park Scientific Instruments, Inc.). The measurement was performed in contact mode using triangle Si_3N_4 cantilevers in air at room temperature. Surface work functions were measured using atmospheric photoelectron spectroscopy (RIKEN Keiki AC-2).

Device fabrication

The bare ITO and SAM-modified ITO were loaded into a bell jar deposition chamber housed in a nitrogen gas glove box. At 10^{-6} Torr, a 50 nm layer of TPD was first deposited, followed by 60 nm of Alq_3 and 1 nm of LiF. Finally, a 70 nm thick aluminium cathode was deposited.

Device characterization

Electroluminescence spectra were obtained with a Minolta CS-1000. The current–voltage and luminance–voltage characteristics were taken with a current–voltage source (Keithley 238) and a Minolta LS-100.

Results and discussion

For the formation of the SAM (Fig. 1), both the Si wafer and the ITO were cleaned by a conventional wet cleaning method.[25,26] The pre-cleaned oxide substrates were immersed in 1 mM anhydrous toluene solution of TPA–CONH–silane for 1 h, followed by thorough rinsing and sonicating in toluene for 5 min. They were then transferred to a 100 °C oven under vacuum for 30 min, after which they were sonicated in toluene again and finally dried under a stream of nitrogen.

Si wafers with native oxide were sometimes used instead of ITO substrates for the convenience of monolayer characterization; because ITO has a rough surface morphology and its transparency is not suitable for surface characterization with, for example, ellipsometry. It has already been reported that both Si wafer and ITO have a similar surface density of reactive sites, about 10^{-6} mol m^{-2}.[27] First, we measured the water contact angles before and after self-assembly. Because the hydroxy groups of the oxide layer generate a hydrophilic surface, both bare Si wafer and bare ITO showed very low water contact angle values ($\theta \ll 15°$), but after self-assembly, relatively high values ($\theta = 77°$ for Si wafer and $\theta = 75°$ for ITO) were observed, indicating that the surfaces of the substrates had become hydrophobic. As well as these contact angle measurements, an XPS study was also performed to investigate the surface atomic composition. Fig. 2 shows the XPS spectra of Si wafers before (lower) and after (upper) self-assembly. Each spectrum was normalized with respect to the peak intensities of abundant elements, that is, Si 2p for Si wafers. Increases in the C 1s (284 eV) and N 1s (410 eV) peak intensities confirmed the formation of a SAM composed of carbon, nitrogen, hydrogen and oxygen. In addition to the above two experiments, the thickness of the SAM

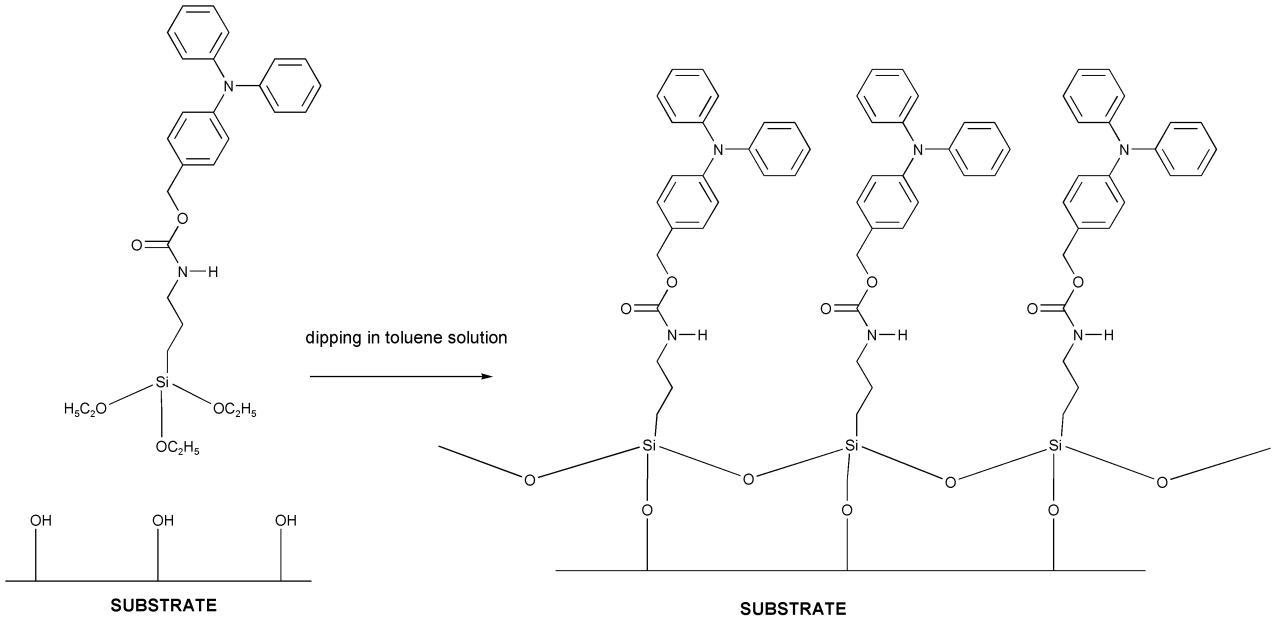

Fig. 1 SAM formation.

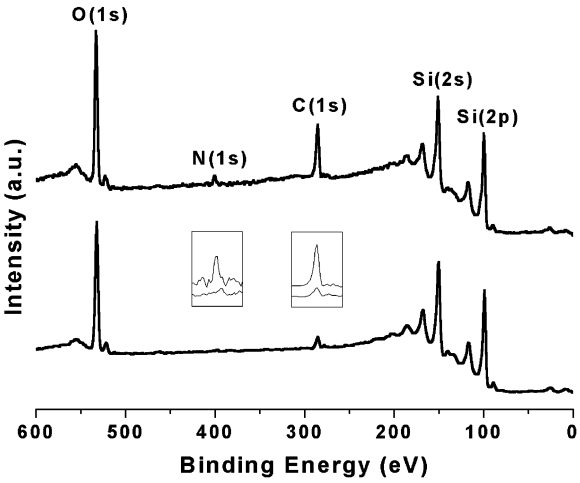

Fig. 2 XPS spectra of Si wafers: upper, TPA–CONH–silane SAM; lower, bare.

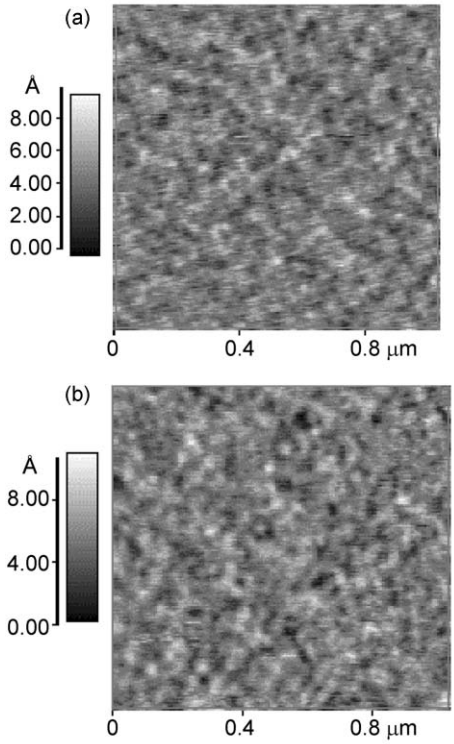

Fig. 3 AFM images of: (a) bare Si wafer; and (b) SAM-modified Si wafer.

was measured by optical ellipsometry. The thickness of the TPA–CONH–silane SAM on the Si wafer was 17 Å, and the distance between the Si atom and a proton of the benzene ring in a fully extended TPA–CONH–silane molecule was calculated to be 18.35 Å.[28] This implies that a layer of monomolecular scale had successfully formed. The surface roughness was confirmed by an AFM study of the Si wafers. Fig. 3 shows the AFM images of a bare Si wafer and a SAM-modified Si wafer. The observed RMS roughness before and after self-assembly was nearly identical, 1.03 Å for the bare Si wafer (Fig. 3(a)) and 1.21 Å for the SAM-modified Si wafer (Fig. 3(b)), indicating that a uniform and flat monolayer is formed during the self-assembly process. We also measured the surface work function values of the ITO substrates using atmospheric photoelectron spectroscopy. The bare ITO exhibited a surface work function of 4.80 eV, but the SAM-modified ITO exhibited a value of 5.30 eV, which indicates that the surface work function of the anode had changed as a result of the SAM formation. This measured value coincides with the HOMO level of TPA–CONH–silane, 5.33 eV, determined electrochemically using cyclic voltammetry (CV).[29] The surface characterization results are summarized in Table 1.

To investigate the effect of the SAM on the OLED device

Table 1 Monolayer characterization results

	Bare	SAM
Water contact angle/°	$\ll 15$	77
	$\ll 15^a$	75^a
Ellipsometry/Å	—	17
RMS roughness[b]/Å	1.03	1.21
Surface work function[a]/eV	4.8	5.3

[a]Values are for ITO rather than Si wafers. [b]Scanning region is a square of 1 μm × 1 μm.

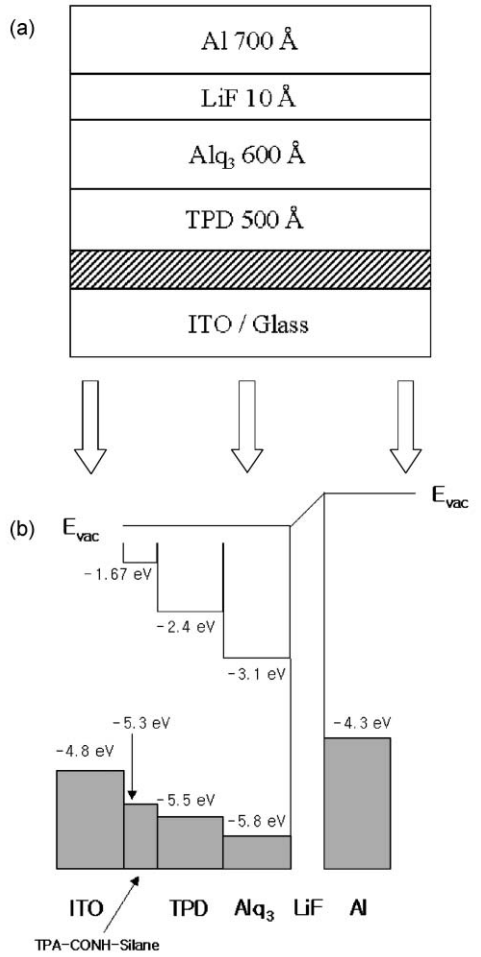

Fig. 4 (a) OLED device configuration. (b) Energy band diagram of the device.

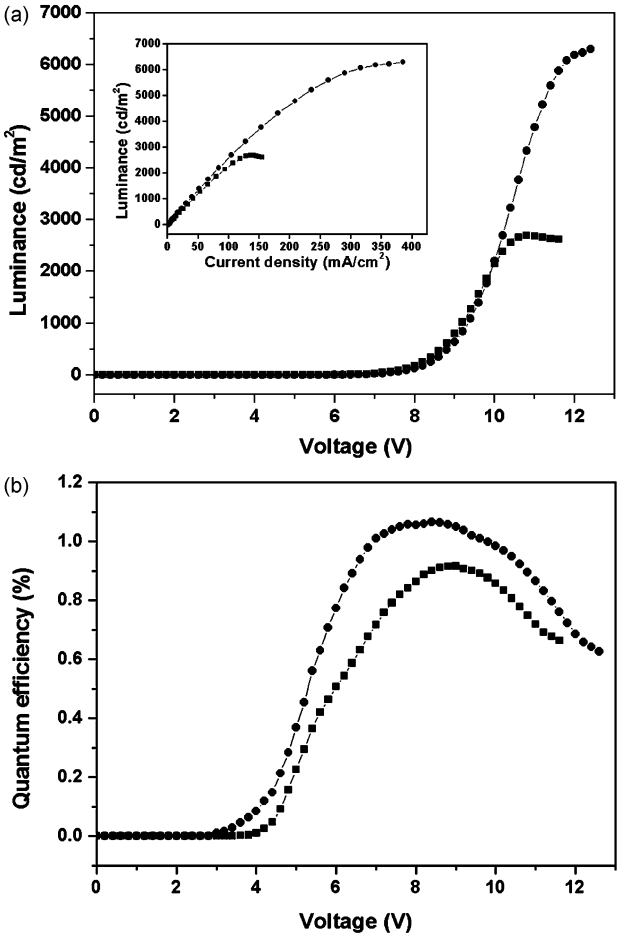

Fig. 5 Device characteristics (●, SAM-modified device; ■, control device): (a) luminance–voltage diagram (inset: luminance–current density diagram); (b) quantum efficiency–voltage diagram.

characteristics, a typical OLED device (SAM-modified ITO/TPD (50 nm)/Alq_3 (60 nm)/LiF (1 nm)/Al (70 nm)) was fabricated, where TPD is the hole-transporting material and Alq_3 the emitting and electron-transporting material (Fig. 4(a)). For comparison, a control device using bare ITO was fabricated at the same time. Both devices showed Alq_3 emission of 525 nm. Fig. 5(a) shows the luminance–voltage diagram of the devices. Although the devices exhibit similar threshold turn-on voltages, the SAM-modified device shows much higher brightness, 6300 cd m^{-2}, compared with that of the control device, 2700 cd m^{-2}. The inset of Fig. 5(a) clearly shows the difference between the two devices. The current limit of the control device is 150 mA cm^{-2}, while the SAM-modified device can endure more than two times higher current, 390 mA cm^{-2}. This is why the SAM-modified device shows higher brightness than the control device. In addition to this durability effect, Fig. 5(b) shows an enhancement of the external quantum efficiency of the SAM-modified device compared with the control device. A maximum external quantum efficiency of 1.1% was measured in the SAM-modified device, compared to 0.92% in the control device. As mentioned earlier, in the discussion of the surface characterization, the SAM-modified ITO has a surface work function of 5.30 eV. Fig. 4(b) shows the energy band diagram of the device. An energy level difference between the ITO anode and the TPD of 0.7 eV is quite a high barrier for hole injection, so the presence of a hole-transporting SAM reduces this barrier to facilitate hole injection and consequently enhances the quantum efficiency of the device.

In order to assess the durability of the device, the effect of the SAM on the interfacial morphology[30] between the ITO anode and the deposited TPD films was further studied. TPD is the most widely used hole-transporting material in OLED fabrication, but the relatively low glass-transition temperature (T_g) of TPD (59–60 °C) is a disadvantage. Because the passage of current during device operation leads to a temperature rise, low T_g organic films are subject to morphology change. Fig. 6(a) and (b) show the SEM images of TPD films deposited on bare ITO substrates before and after heating at 80 °C for 1 h, respectively. Fig. 6(c) is for a SAM-modified ITO substrate after heating at 80 °C for 1 h. As can be seen, bare ITO shows dewetting of the TPD molecules on heating whereas the SAM-modified ITO maintains perfect wetting of the TPD and a flat surface morphology. The dewetting of the TPD means that when the LED device is operating, pinhole formation is accelerated with increased dewetting of the TPD. The perfect wetting of the SAM-modified ITO is due to the structural similarity of the terminal groups of the SAM and of the deposited TPD molecules. Therefore it has been shown that interface compatibility problems can be solved through organic SAM formation.

Although an improvement in the performance of the OLED device was proved as a result of a SAM, the constant device turn-on voltage is still open to further discussion. There are two kinds of effect of SAM-modification on the device characteristics. One is the change of device turn-on voltage, by lowering the threshold of charge injection, and the other is the improvement of interfacial contact between the electrode and organics. In our case, the HOMO values of TPA and of TPD are not significantly different to lower the turn-on voltage

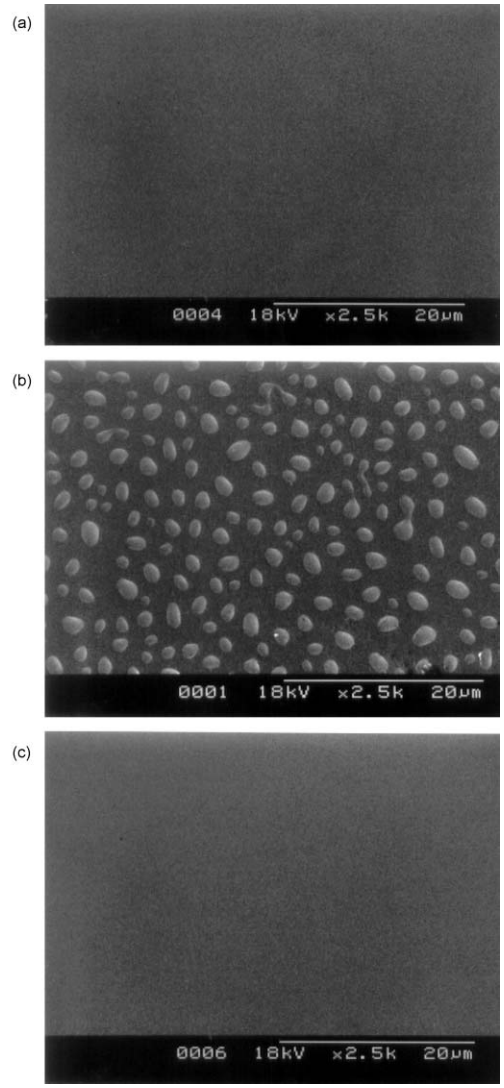

Fig. 6 SEM images of TPD deposited on ITO. (a) Bare ITO before thermal annealing. (b) Bare ITO after thermal annealing at 80 °C for 1 h. (c) SAM-modified ITO after thermal annealing at 80 °C for 1 h.

drastically but the effect of contact improvement is rather influential. So the modified device could endure a higher current and showed a higher brightness. Variation of the terminal group of the SAM to control charge injection is under investigation.

Conclusion

An ethoxysilane functionalized hole-transporting triphenylamine (TPA–CONH–silane) was synthesized and this was self-assembled to form a monolayer on the ITO anode. Various aspects of SAM formation were characterized and an OLED device based on a SAM-modified ITO was fabricated. The SAM-modified device could endure higher current and showed much higher luminance than the bare ITO device. External quantum efficiency as well as maximum luminance was shown to improve as a result of SAM formation. A study of the TPD film morphology revealed an enhanced thermal stability of the device modified with the SAM. The variation of the terminal group of the SAM and possible further optimization of the SAM-modified OLEDs is under investigation.

Acknowledgements

This work was supported by the Center for Advanced Functional Polymers (CAFPoly) through KOSEF and the Ministry of Information and Communications (MIC), Republic of Korea.

References and notes

1 (*a*) C. H. Chen, J. Shi and C. W. Tang, *Macromol. Symp.*, 1998, **125**, 1; (*b*) U. Mitschke and P. Bäuerle, *J. Mater. Chem.*, 2000, **10**, 1471.
2 (*a*) A. Kraft, A. C. Grimsdale and A. B. Holmes, *Angew. Chem. Int. Ed.*, 1998, **37**, 402; (*b*) H. K. Shim and J. I. Jin, *Adv. Polym. Sci.*, 2002, **158**, 194.
3 P. E. Burrows, V. Bulovic, S. R. Forrest, L. S. Sapochak, D. M. McCarty and M. E. Thompson, *Appl. Phys. Lett.*, 1994, **65**, 2922.
4 E. M. Han, L. M. Do, Y. Niidome and M. Fujihira, *Chem. Lett.*, 1994, **5**, 969.
5 E. Bellmann, G. E. Jabbour, R. H. Grubbs and N. Peyghambarian, *Chem. Mater.*, 2000, **12**, 1349.
6 T. D. Morais, F. Chaput, K. Lahlil and J.-P. Boilot, *Adv. Mater.*, 1999, **11**, 107.
7 J. E. Malinsky, G. E. Jabbour, S. E. Shaheen, J. D. Anderson, A. G. Richter, T. J. Marks, N. R. Armstrong, B. Kippelen, P. Dutta and N. Peyghambarian, *Adv. Mater.*, 1999, **11**, 227.
8 J. Cui, A. Wang, N. L. Edleman, J. Ni, P. Lee, N. R. Armstrong and T. J. Marks, *Adv. Mater.*, 2001, **19**, 1476.
9 A. Ulman, *Chem. Rev.*, 1996, **96**, 1533.
10 A. Berlin, G. Zotti, G. Schianon and S. Zecchin, *J. Am. Chem. Soc.*, 1998, **120**, 13453.
11 S. F. J. Appleyard, S. R. Day, R. D. Pickford and M. R. Willis, *J. Mater. Chem.*, 2000, **10**, 169.
12 Y. Koide, Q. Wang, J. Cui, D. D. Benson and T. J. Marks, *J. Am. Chem. Soc.*, 2000, **122**, 11266.
13 B. Choi, J. Rhee and H. H. Lee, *Appl. Phys. Lett.*, 2001, **79**, 2109.
14 R. A. Hatton, S. R. Day, M. A. Chesters and M. R. Willis, *Thin Solid Films*, 2001, **394**, 292.
15 E. L. Bruner, N. Koch, A. R. Span, S. L. Bernasek, A. Kahn and J. Schwartz, *J. Am. Chem. Soc.*, 2002, **124**, 3192.
16 P. K. H. Ho, J.-S. Kim, J. H. Burroughes, H. Becker, S. F. Y. Li, T. M. Brown, F. Cacialli and F. R. Friend, *Nature*, 2000, **404**, 481.
17 C.-G. Wu, H. T. Hisao and Y.-R. Yeh, *J. Mater. Chem.*, 2001, **11**, 2287.
18 L. A. J. Chrisstoffels, A. Adronov and J. M. J. Fréchet, *Angew. Chem. Int. Ed.*, 2000, **39**, 2163 and references cited therein.
19 J. Collet, O. Tharaud, A. Chapotonm and D. Vuillaume, *Appl. Phys. Lett.*, 2000, **76**, 1941.
20 J. H. Schön, H. Meng and Z. Bao, *Adv. Mater.*, 2002, **14**, 323.
21 J. Naciri, J. Y. Fang, M. Moore, D. Shenoy, C. S. Dulcey and R. Shashidhar, *Chem. Mater.*, 2000, **12**, 3288.
22 U. Srinivasan, M. R. Houston, R. T. Howe and R. Maboudian, *J. Microelectromech. Syst.*, 1998, **7**, 252.
23 K. J. Moon, H. K. Shim, K. S. Lee, J. Zieba and P. N. Prasad, *Macromolecules*, 1996, **29**, 861.
24 R. S. Clegg and J. E. Hutchson, *Langmuir*, 1996, **12**, 5239.
25 P. K. H. Ho, M. Granström, R. H. Friend and N. C. Greenham, *Adv. Mater.*, 1998, **10**, 769.
26 Z. Q. Wei, C. Wang, C. F. Zhu, C. Q. Zhou, B. Xu and C. L. Bai, *Surf. Sci.*, 2000, **459**, 401.
27 (*a*) J. H. Moon, J. H. Kim, K.-J. Kim, T.-H. Kang, B. Kim, C.-H. Kim, J. H. Hahn and J. W. Park, *Langmuir*, 1997, **13**, 4305; (*b*) S.-Y. Oh, Y.-J. Yun, D.-Y. Kim and S.-H. Han, *Langmuir*, 1999, **15**, 4690.
28 The calculation was performed with CS Chem3D Pro software using an MM2 energy minimization method. Refer to Electronic Supplementary Information†.
29 CV was performed on an AUTOLAB/PGSTAT12 with a three-electrode cell in a solution of Bu_4NBF_4 (0.10 M) in acetonitrile at a scan rate of 50 mV s^{-1}. The HOMO level of the compound was calculated regarding the oxidation potential of ferrocene as −4.80 eV.
30 (*a*) S. Goncalves-Conto, M. Carrard, L. Si-Ahmed and L. Zuppiroli, *Adv. Mater.*, 1999, **11**, 112; (*b*) J. Cui, Q. Huang, Q. Wang and T. J. Marks, *Langmuir*, 2001, **17**, 2051.